PHYSICAL REVIEW B VOLUME 62, NUMBER 15 15 OCTOBER 2000-I

Three-dimensional global optimization of $\mathrm{Na}_n{}^+$ sodium clusters in the range $n \leqslant 40$

F. Calvo,* S. Tran, S. A. Blundell, and C. Guet
Département de Recherche Fondamentale sur la Matière Condensée, Service des Ions, Atomes et Agrégats, CEA Grenoble, 17 rue des Martyrs, F-38054 Grenoble Cedex, France

F. Spiegelmann
Laboratoire de Physique Quantique, IRSAMC, Université Paul Sabatier, 118 Route de Narbonne, F-31062 Toulouse Cedex, France

(Received 22 March 2000)

Likely candidates for the ionic structure and lowest-energy minima of cationic sodium clusters $\mathrm{Na}_n{}^+$ are presented in the size range $n = 4-40$. We perform a systematic and unconstrained global optimization by the basin-hopping method with three different energy functions: a many-body empirical classical potential modified to account for the extra ionic charge, a simple quantal Hückel-type model, and a density-functional-theory-based orbital-free model. The similarities and differences between the models are discussed, and the global shapes are analyzed with the Hill-Wheeler parameters.

I. INTRODUCTION

Because of the fundamental interest in understanding how metallic properties built up in finite systems and because they exhibit the simplest valence electronic structure among all metals, alkali-metal clusters have been, since the pioneering experiments of Knight *et al.*,[1] the object of intense experimental and theoretical attention.[2–4] Although the simple spherical jellium model[5,6] proved to be successful in explaining many properties related to the so-called electronic shell stability in the range from a few tens to a few hundreds of atoms, it has appeared that, despite the important screening and the leading role of the electrons in the stability, properties of alkali-metal clusters are significantly influenced by the actual shape and geometrical arrangements of nuclei. For instance, the relationship between geometrical structures and optical spectra has been widely discussed.[4,7–9] Moreover, recent experiments[10] concerned with thermodynamical behavior have used the optical signatures of alkali-metal clusters to pinpoint the influence of temperature, stressing the transition from a rigidlike molecular-type behavior regime to a liquidlike or melted regime. Thus, even in the case of simple metal clusters, the geometric factors are significant and the knowledge of the equilibrium geometries of the low-lying isomers is important.

Various directions have been pursued in order to include the shape and/or ionic structure more or less explicitly in theoretical investigations. In principle, *ab initio* calculations performed by Hartree-Fock plus configuration interaction[9,11,12] or density-functional theory[13–15] methods are certainly the most reliable and accurate in determining the forces acting on the nuclei and in obtaining the lowest-energy isomers. Alkali-metal clusters present a rather favorable case since the electronic problem can be rather safely restricted to the valence metallic electrons via the use of adequate effective atomic core potentials or pseudopotentials.

For sodium clusters including less than, say, 20 atoms, such *ab initio* calculations were performed[9,11–14,16] and have proposed low-lying equilibrium structures. However, the combination of such accurate calculations with optimization algorithms in order to find the minimal energy configuration on some complex potential-energy surface turns out to be a difficult task, especially in the case of clusters where numerous secondary minima exist. Usually, the search of minima has been performed using gradient techniques at the Hartree-Fock or coupled-cluster level, or by simulated annealing techniques combining the density functional theory with a Car-Parinello approach.[13,14] However, such search algorithms are known not to be always successful in finding the global minimum and the situation worsens quickly as the number of atoms exceeds a few tens.

Indeed, clusters are now commonly considered as a benchmark for testing global optimization algorithms.[17–20] In particular, many efforts have been devoted to the optimization of Lennard-Jones (LJ) clusters, for which several highly non trivial geometries can be found in the range of less than 100 atoms.[21,22] The example of Lennard-Jones clusters has shown that the determination of the global minima can be very tricky even in the case of pairwise interactions and only a few tens of atoms. Although there is no actual entirely safe and fullproof technique that ensures to find the actual global minimum, some recent global algorithms such as the ''basin-hopping'' technique developed by Wales and Doye[23] or the genetic algorithms[24] have demonstrated their efficiency and in many cases their use is necessary. Obviously the use of global techniques also imply an extensive sampling of the potential energy surface and cannot yet be at present combined with fully *ab initio* techniques, even though constant progresses are made to speed up the electronic calculations, like for instance the developments of algorithms scaling linearly with size.

Various schemes have been developed to reduce the system complexity and to deal with ionic structure and shape isomerism in a larger size range, up to a few tens. Several approaches restrict the number of degrees of freedom associated with the positions of the nuclei and consider only global shapes of clusters, parametrized via deformation coordinates. The spheroidal jellium approximation was developed by Eckardt and Penzar within the self-consistent local-

0163-1829/2000/62(15)/10394(11)/$15.00

density approximation (LDA) scheme.[25] Further extensions of the jellium model including the lowest-order multipolar deformations such as the structure averaged jellium model[26–29] (SAJM) or the ellipsoidal jellium model[30–33] were also investigated treating the electrons either via the LDA or some corrected Thomas-Fermi type approximations. Whereas the above models still rely on the continuous background approximation, the number of degrees of freedom is drastically reduced and remains constant with size. Another interesting approach was provided by the use of pseudopotentials in constrained local density schemes implying spherically averaged pseudopotentials[34] (SAPS) or more realistically cylindrically averaged pseudopotentials (CAPS).[8,35,36] However, whereas the latter methods fix no constraint on the nuclei, the spherical or cylindrical average of the ionic potential seen by the electrons may yield some bias and prevent from finding a true three-dimensional (3D) minimum, especially in open-shell situations.

Other approaches keep the full complexity related to the nuclear degrees of freedom but simplify the level of treatment of the electronic problem without imposing *a priori* global symmetry constraints. Various approximations and models have been proposed and used. The present work situates in this context and intends to compare and discuss in the size range of 4–40 atoms the 3D globally optimized structures of singly positively charged sodium clusters obtained with different models to represent the atomic cohesion. The lowest level of treatment is clearly associated with the use of classical potentials, mainly with embedded-atom type potentials, which in the case of metal clusters are the most commonly used expressions. Even more approximative Morse pairwise potentials have also been proposed in the past.[37] We have also considered the tight-binding scheme which can be considered as the simplest approximation of a linear combination of atomic orbtals (LCAO) quantum approach and was found to produce realistic structures for neutral clusters at least in the range of 2–20 atoms where comparison could be made with more sophisticated calculations previously reported. Finally we investigate the semiclassical approach relying up on extensions of the Thomas-Fermi scheme, which was already mentioned above in the jellium model context but which can also be used with explicit discrete ions and atom-based pseudopotentials.[38] It is similar to the orbital-free model previously used in several clusters studies.[39] An interest of this model is that it allows the study of charged (even multicharged) clusters with no modifications.[38] Obviously any of these methods might fail because of the approximations assumed. However, they provide sufficiently fast calculations of the potential-energy function so that they can actually be combined with efficient global three-dimensional unconstrained optimization algorithms in the size range 10–50.

We thus report a systematic comparison of 3D globally optimized structures of $\mathrm{Na}_n{}^+$ clusters described by the three models. We have combined these models with the basin-hopping global optimization algorithm, which was proved to be extremely efficient in the case of clusters and easy to implement and requiring no *a priori* guiding lines about the cluster construction as it was used sometimes in other successful optimization schemes such as genetic algorithms. The scope is fourfold: (i) to obtain reliable geometrical databases in the different models for this class of clusters; (ii) to discuss the validity of the various models, their similarities and their peculiarities with respect to the physics involved in the light of more sophisticated calculations when available; (iii) to investigate the morphologic properties and building sequences in an extended size range; and (iv) to discuss the possible influence of the charge in the different models. Although we have performed similar investigations for the neutral clusters, the emphasis is put here on positively charged clusters. Partially, the results for neutral clusters have already been discussed elsewhere.[40,41]

II. ENERGY FUNCTIONS AND OPTIMIZATION METHODS

At the scale of the sizes investigated here, $n \leqslant 40$ atoms, the three models will be presented in order of their increasing computational complexity, namely from an empirical model to a semiclassical model via a quantum one. The first simplest model was chosen in order to perform nearly exhaustive global optimization up to 40 atoms. It consists of a many-body classical potential of the Gupta type.[42] A larger class of such potentials for metallic systems is the famous embedded-atom model (EAM) family.[43] The Gupta potential is based on the second-moment approximation (SMA) of the density of states in a tight-binding model.[44] In the SMA models, the total energy of a neutral system with n atoms located at $\{\mathbf{r}_i\}$ is calculated as

$$E(\{\mathbf{r}_i\}) = \sum_i \ \varepsilon_0 \sum_{j\neq i} \ \exp\left[p\left(1-\frac{r_{ij}}{r_0}\right)\right] - \sum_i \ \left\{\zeta_0^2 \sum_{j\neq i} \ \exp\left[2q\left(1-\frac{r_{ij}}{r_0}\right)\right]\right\}^{1/2}. \tag{1}$$

Such a potential was previously used by many authors for metal clusters.[40,41,45–49] Recently, another type of embedded-atom parametrization for LJ solids has been proposed by Baskes.[50] The effect of charging the cluster in this empirical potential is, in principle, difficult to account for, because the missing electron should be treated as a continuous one. A simple model of the same level of approximation can be built by assuming a single positive partial charge q_i on each nucleus. The charges then interact through electrostatic and polarization forces. Such a model, with an uniform charge distribution over the volume and with scalar polarization forces $(1/r^4)$ was employed by Li and co-workers[51] to study a Coulomb fragmentation of multiply charged sodium clusters. However, there are few problems in this crude model that can be easily solved. First, if the same values of the parameters ε_0 and ζ_0 are taken for both the neutral and the charged clusters, then ionic clusters are found to be less bound than their neutral counterparts, which is in contradiction with experimental data.[52–54] We have slightly modified these parameters in order to account for this discrepancy by setting[40]

$$\varepsilon_0^+ = c\varepsilon_0, \quad \zeta_0^+(n) = c\zeta_0(1+a/n^b) \tag{2}$$

as new size-dependent parameters, with the values $a=6.6$, $b=1.27$ and $c=1.0055$. A second problem comes from the metallic nature of sodium clusters. In such systems, the charge is located mostly on the surface and not homogeneously over the entire volume. To mimic this effect in the charge distribution, we have used the simple model recently reported in Ref. 55. This model is built upon a simple observation that surface atoms are less bound but more charged. In this scheme, an individual partial charge q_i is related to an estimate v_i of the binding energy of a nucleus i via an empirical function F:

$$q_i = QF(v_i) \bigg/ \sum_j F(v_j), \tag{3}$$

where Q is the total charge of a cluster. In order to facilitate computations of the forces, v_i is taken as a Morse potential: $v_i = \Sigma_{j\neq i} w_{ij}(w_{ij}-2)$ with $w_{ij} = \exp[\rho(1-r_{ij}/r_0)]$, and F is chosen as a Fermi function

$$F(v) = \left[1 + \exp\left(\frac{v_0 - v}{\Delta v}\right)\right]^{-1}. \tag{4}$$

Once the charges are known for a given ionic configuration, we add the Coulombic contribution to the energy in a similar way as in Refs. 51, but with more realistic vector polarization forces:

$$\begin{aligned} E^+(\{\mathbf{r}_i\}) = {} & \sum_i \varepsilon_0^+ \sum_{j\neq i} \exp\left[p\left(1 - \frac{r_{ij}}{r_0}\right)\right] \\ & - \sum_i \left\{(\zeta_0^+)^2 \sum_{j\neq i} \exp\left[2q\left(1 - \frac{r_{ij}}{r_0}\right)\right]\right\}^{1/2} \\ & + \frac{1}{2}\sum_i \sum_{j\neq i} \frac{q_i q_j}{r_{ij}} - \frac{1}{2}\sum_i \alpha_i \mathbf{E}_i^2. \end{aligned} \tag{5}$$

In this equation, $\mathbf{E}_i$ is an electrostatic field created by all point charges outside $\mathbf{r}_i$, and $\alpha_i = 1.01$ a.u. is the polarizability on site i. The parameters ε_0, ζ_0, p, q, and r_0 of the cohesive energy were taken as those proposed by Li *et al.*:[51,56] $\varepsilon_0 = 1.5955\times 10^{-2}$ eV, $\zeta_0 = 0.291\,13$ eV, $p = 10.13$, $q = 1.30$, and $r_0 = 6.99a_0$. These parameters were fitted only for bulk properties, and we are aware that this model should, therefore, be taken cautiously when used for clusters.[57]

The parameters ρ, v_0, and Δv of the electrostatic model described by Eqs. (3) and (4) were fitted to more sophisticated density-functional theory (DFT) calculations at a finite temperature on the large charged cluster Na_{274}^{8+} at 345 K.[38] Good agreement was found for the values $\rho = 4.194$, $v_0 = -6.6$, and $\Delta v = 1.6$. This empirical model is computationally simple enough so that local optimizations beginning with an arbitrary structure are relatively cheap. This allowed us to use powerful global optimization algorithms to find the lowest-energy geometries of $\mathrm{Na}_n{}^+$ clusters. Our choice was the so-called basin-hopping method of Wales and Doye,[23] already used for very different systems.[22,58] Briefly, this method belongs to hypersurface deformation methods, and an initial surface $E(\mathbf{R})$ undergoes a staircase transformation toward a new energy surface $\tilde{E}(\mathbf{R}) = \min\{E(\mathbf{R})\}$, where min indicates that a local minimization is performed starting with configuration $\mathbf{R}$. A simple Metropolis Monte Carlo (MC) algorithm is used to explore the surface $\tilde{E}$ where the global minimum is to be found. The success of this method is related to the fact that all barriers on the initial surface vanish after deformation. Therefore, very large MC steps can be used to sample $\tilde{E}$ with respect to their value in a common simulated annealing process. Other types of deformations of the energy landscape have been proposed, as in the recent stochastic tunneling approach of Wenzel and Hamacher.[59] For each size in the range $4\leqslant n\leqslant 40$, 5×10^4 quenches were carried out during the basin-hopping search.

Our second model was developed initially for neutral sodium clusters,[60] and parametrized for reproducing molecular properties of Na_2 and Na_4 only. It consists of a distance-dependent tight-binding (DDTB, or hereafter simply TB) quantal Hamiltonian $\hat{h}$ given by

$$\hat{h} = \sum_{ij} h_{ij} a_i{}^\dagger a_j, \tag{6}$$

where $a_i{}^\dagger$ and a_j are creation and annihilation operators corresponding to an s orbital on nucleus i or j, respectively. The effect of p orbitals is included in a perturbative way in the matrix elements:

$$h_{ii} = h_{ii}^{(0)} + h_{ii}^{(2)} = \sum_{k\neq i}\left[\rho_{ss}(r_{ik}) - \frac{t_{s\sigma}^2(r_{ik})}{\varepsilon_{3p} - \varepsilon_{3s}}\right], \tag{7}$$

$$h_{ij} = h_{ij}^{(0)} + h_{ij}^{(2)} = t_{ss}(r_{ij}) - \sum_{k\neq i,j}\left[\frac{t_{s\sigma}(r_{ik})t_{s\sigma}(r_{jk})}{\varepsilon_{3p} - \varepsilon_{3s}}\,\frac{\mathbf{r}_{ik}\cdot\mathbf{r}_{jk}}{\|\mathbf{r}_{ik}\|\|\mathbf{r}_{jk}\|}\right], \tag{8}$$

$\rho_{ss}(r)$, $t_{ss}(r)$, and $t_{s\sigma}(r)$ being the respective ion-ion repulsion and the s-s and s-p_σ transfer integrals. These functions were taken as dependent of interatomic distances. The total energy of the electronic ground state is calculated for a given ionic configuration as the sum of one-electron energies of the occupied orbitals:

$$E = \sum_{i\in \mathrm{occ}} n_i \varepsilon_i. \tag{9}$$

Here, ε_i's are the eigenvalues of the Hamiltonian and n_i's are the occupation numbers. This model was previously used in many investigations ranging from geometrical[61] to dynamical[62] and thermodynamical[41,63–65] studies. For neutral clusters, it has been shown to provide low-energy structures in very good agreement with *ab initio* configuration interaction and density-functional studies.[13,14,66] It may nevertheless underestimate stabilities at shell closings, despite a generally correct behavior and the reproduction of odd/even size alternations.[67]

The tight-binding model can easily deal with singly charged clusters, by simply modifying the occupation numbers in summing the orbital energies. The charge distribution on the atoms in the cluster is thus only governed by delocalization of the emptied orbital. It should be mentioned that there is no explicit electrostatic balance, and the electron-electron repulsion is not accounted for at all. Because the diagonalization of a $n\times n$ matrix is required for each computation of the energy, this quantal model, albeit simple, is numerically more expensive than the empirical SMA model. In particular, the cost grows with size nearly as its cube, which is a serious limitation for large clusters. For this reason we had to reduce the number of local optimizations in the basin-hopping search down to 5000.

In an extended-Thomas-Fermi (ETF) approximation, the ions are still represented by discrete masses, but the valence electrons are treated explicitly. To each ionic configuration $\mathbf{R}=\{\mathbf{r}_i\}$ corresponds an electronic density $\rho(\mathbf{r})$ which can be used, in turn, to calculate the forces acting on the ions. In this model, the potential energy E is written as the functional of the density ρ and the ionic coordinates $\{\mathbf{r}_i\}$:[38]

$$E[\rho,\{\mathbf{r}_i\}]=E_{\mathrm{TF}}[\rho]+E_{\mathrm{W}}[\rho]+E_{\mathrm{H}}[\rho]+E_{\mathrm{XC}}[\rho]+E_{\mathrm{I}\text{-}I}[\{\mathbf{r}_i\}] + E_{\mathrm{I}\text{-}\mathrm{e}}[\rho,\{\mathbf{r}_i\}]. \tag{10}$$

The different terms in the latest expression are briefly reviewed as follows. $E_{\mathrm{TF}}[\rho]$ is the electron kinetic energy in the Thomas-Fermi approximation, which takes the form

$$E_{\mathrm{TF}}[\rho]=\frac{3}{10}(3\pi^2)^{2/3}\int \rho^{5/3}d^3\mathbf{r}. \tag{11}$$

The Weizsäcker term E_{W} gives the first-order gradient correction to $E_{\mathrm{TF}}[\rho]$ to take into account, for inhomogeneities in the electron density:

$$E_{\mathrm{W}}[\rho]=\frac{\lambda_{\mathrm{W}}}{72}\int \frac{(\nabla\rho)^2}{\rho}d^3\mathbf{r}, \tag{12}$$

where the constant λ_{W} is taken as 1.44 au. The electron-electron interactions are given by the usual Hartree term

$$E_{\mathrm{H}}[\rho]=\frac{1}{2}\int \frac{\rho(\mathbf{r})\rho(\mathbf{r}')}{\|\mathbf{r}-\mathbf{r}'\|}d^3\mathbf{r}\,d^3\mathbf{r}', \tag{13}$$

plus an exchange-correlation functional in the local-density approximation:

$$E_{\mathrm{XC}}[\rho]=-\frac{3}{4}\left(\frac{3}{\pi}\right)^{1/3}\int \rho^{4/3}d^3\mathbf{r}+E_{\mathrm{C}}[\rho]. \tag{14}$$

The Gunnarsson and Lundqvist parametrization[68] was chosen for the correlation function $E_{\mathrm{C}}[\rho]$. The ion-ion interaction $E_{\mathrm{I\text{-}I}}[\{\mathbf{r}_i\}]$ is taken to be just the Coulomb interaction between ions Na^+ i and j. Finally, the ion-electron interaction is modeled by a local and spherically symmetric pseudopotential $V_{\mathrm{ps}}(r)$ to mimic the interaction between a valence electron and an ion core,

$$E_{\mathrm{I}\text{-}e}[\rho,\{\mathbf{r}_i\}]=\int \rho(\mathbf{r})V_{\mathrm{ion}}(\{\mathbf{r}_i\},\mathbf{r})d^3\mathbf{r}, \tag{15}$$

$$V_{\mathrm{ion}}(\{\mathbf{r}_i\},\mathbf{r})=\sum_i V_{\mathrm{ps}}(\|\mathbf{r}-\mathbf{r}_i\|). \tag{16}$$

We have used a ''flat'' pseudopotential given, for $r'=\|\mathbf{r}-\mathbf{r}_i\|$, by

$$V_{\mathrm{ps}}(r')=\begin{cases}-1/r', & r'>r_n\\ -\dfrac{1}{6r_n}\left[7-\left(\dfrac{r'}{r_n}\right)^6\right], & r'\leqslant r_n\end{cases} \tag{17}$$

with the value $3.55a_0$ for the cutting radius r_n. This model was used with a real-space grid, for which the flat pseudopotential is computationally cheaper. The grid step h was taken as a_0, larger values leading to numerical uncertainties make difficult the separation in energy between close isomers. Since there are no explicit shell effects nor orbitals in this model, its cost roughly increases linearly with size. However, in the size range considered here, it is still much more expensive than the TB model due to the continuous representation of the electronic density. Systematic and unconstrained global optimization in the same way as with the previous models thus appeared to be impossible at the same scale. We have instead chosen a ''semiglobal'' approach where only databases of structures generated by other models were locally reoptimized in the ETF model. Assuming that the energy landscapes bear some similarities, we can perform each local optimization only once instead of possibly hundreds of times by standard basin-hopping. Of course, the price we pay for this bias is that some important structures may be missed because of the differences in the energy landscapes. In the present case, however, we believe that this approach remains fruitful, as we shall see below. Among all isomers collected after a basin-hopping search for any given size and model, we kept the 100 lowest in energy for local optimization in the ETF model.

III. RESULTS AND DISCUSSION

The lowest-energy geometrical configurations of the $\mathrm{Na}_n{}^+$ clusters found by the basin-hopping algorithm or by a local reoptimization are presented in Fig. 1 for the three energy functionals. The corresponding binding energies and point groups are given in Table I. The particular stability of some sizes is emphasized in Fig. 2, where we plotted the total energy relative to a fit on liquid drop like model of the form $E(N)=a+bN^{1/3}+cN^{2/3}+dN$. In the bottom panel of this figure, we also presented the relative stability of each cluster with respect to its neighbors, quantified by $\Delta_2E(N)=E(N+1)+E(N-1)-2E(N)$.

Morphologies predicted by the empirical SMA potential have many similarities with the global minima of pairwise Lennard-Jones clusters. At low sizes, the growth sequence leads to an icosahedron at $n=13$, by capping atoms over a seven-atom pentagonal bipyramid. The bipyramid $(n=6)$ and antiprism $(n=8)$ are the only exceptions to this rule. Surprisingly, the growth over the primitive icosahedron does not follow immediately the same rules found for LJ or Morse clusters. While $\mathrm{Na}_{14}{}^+$ and $\mathrm{Na}_{15}{}^+$ are still singly and doubly capped icosahedra respectively, the structure of $\mathrm{Na}_{16}{}^+$ includes some elements of hexagonal symmetry, which were not observed by using other many-body potentials. $\mathrm{Na}_{17}{}^+$ prefers a non-compact geometry, with four capping atoms that minimize electrostatic repulsion. From $n=18$ to $n=40$ atoms, the anti-Mackay, or ''polyicosahedral'' growth sequence is generally found. As the inner pressure becomes too high, larger sizes exhibit preferentially the Mackay growth sequence involving multilayer icosahedra. Only two Mackay-type clusters are seen for $n=39$ and 40 in Fig. 1(a). The special stability of anti-Mackay clusters is also exhibited on Fig. 2(b) by the series of peaks (secondary magic numbers) for $n=19$, 23, 26, 29, and 32.

Only one size above 8 displays a geometry not based on pentagonal or icosahedral symmetry, namely $\mathrm{Na}_{38}{}^+$. This cluster is a truncated octahedron in the SMA model. This very peculiar geometry turns out to be met very often in clusters of this size modeled by simple potentials, the only exception being the Au_{38} cluster in the work by Garzón and co-workers.[69] It has been also observed experimentally among nickel clusters.[70] At the size of $n=28$, the cluster does not exhibit any special symmetry, and looks rather compact. No evidence for close-packed (except the fcc Na_{38}^{+}) or decahedral structure was found for this size range in the SMA model.

We have also investigated the neutral clusters using the SMA potential. Preliminary results have been published elsewhere.[41] For the most sizes in the range 4–40, we found no significant difference in morphology between Na_n (SMA) and Na_n^{+} (SMA), but only some distortions in several cases. Of course, the absence of any quantal character and the decreasing influence of the extra charge should be responsible for this. However, the model of charge distributions that we have used in the present work, in contrast to the homogeneous distribution used in Ref. 41, yields some structural differences for the sizes $n=15$, 17, and 34. In all the cases, the energy gap between two lowest energy isomers found during the global optimization is very small.

The distance-dependent tight-binding model exhibits very different equilibrium geometries in the complete range 4–40. Indeed, only for $n=5$ and 7, and for the larger sizes $n=25$–29, 31–34, the same structures are found in the SMA and TB models. While the growth sequences could be easily identified in the SMA model, we now see a very strong size dependence, especially at low sizes. The global geometry of clusters containing up to about 25 atoms is based on capping isolated atoms over a fivefold symmetric seed. The resulting structures are not compact. Good examples are Na_{13}^{+} or Na_{21}^{+}. For the small clusters, the present geometries resemble those of CI calculations.[9,12] From $n=16$, an icosahedral core sets up and becomes a double icosahedron core with a missing apex atom beyond $n=18$. Although the growth sequence differs from that obtained in the SMA model, anti-Mackay geometries are present systematically for all larger clusters up to 40 atoms. In particular, we do not see any truncated octahedron for $n=38$, neither any decahedral, close-packed or Mackay-type structure in this size range.

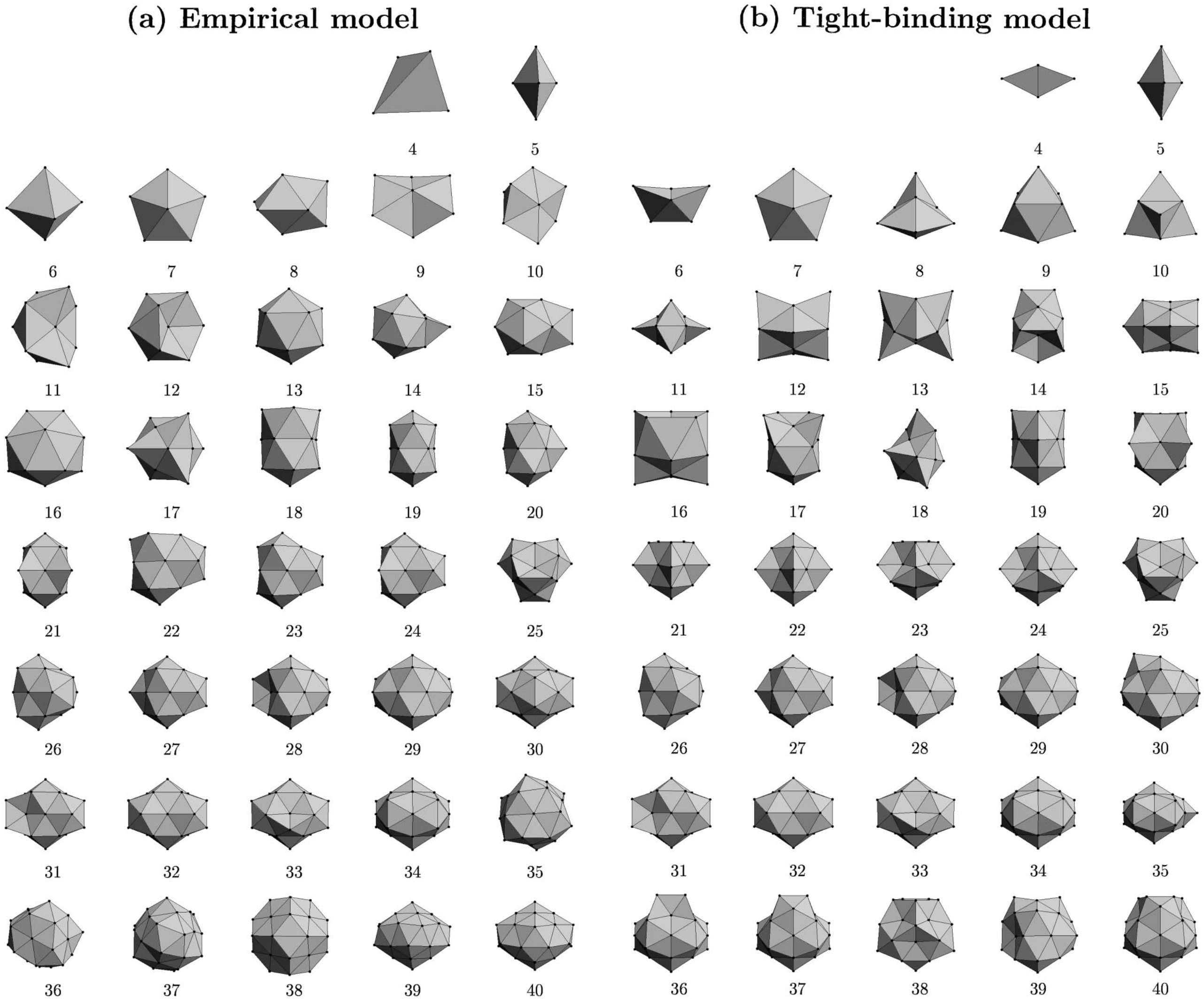
(a) Empirical model

(b) Tight-binding model

FIG. 1. Structures of the Na_n^{+} clusters, $4\leqslant n\leqslant 40$, found by a basin-hopping Monte Carlo minimization (SMA and TBA models) or by a local reoptimization (ETF model). (a) Results in the empirical SMA model; (b) results in the simple quantal TB model; (c) results in the semiclassical ETF model.

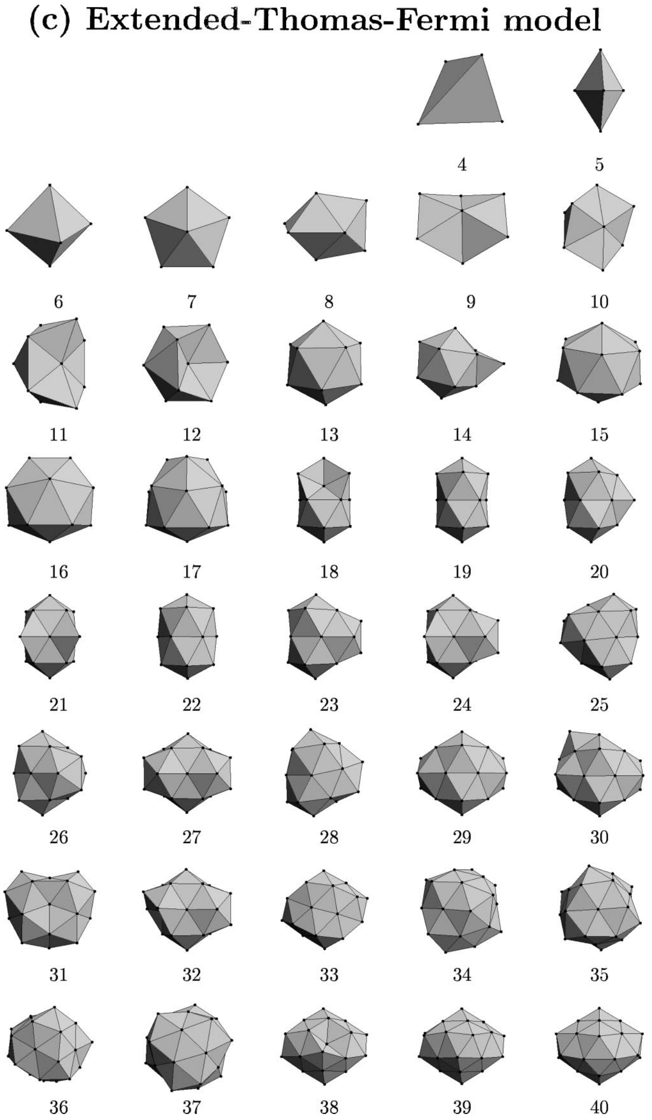

FIG. 1. (*Continued*).

The tight-binding model includes quantal effects explicitely such as the electron delocalization, and the structures found reflect some of these aspects. A striking example is the odd/even alternation in the stabilities that one can observe in the lower part of Fig. 2. Some structures having an even number of valence electrons are thus much more stable than their neighbors. When this occurs along with strongly symmetric ionic geometries, the cluster can be even more stable. This happens for $n=5$, 7, 9, 11, or 29. Not surprisingly, the important variations with size are also reflected on the large deviations with the continuous liquid drop model in Fig. 2(a).

Neutral sodium clusters in the tight-binding model have been considered previously. The geometries obtained by Poteau and Spiegelmann[61] up to the size 40 are very different from those reported here for cationic systems, especially for small clusters where the effect of an extra charge is expected to be more prominent. The growth algorithm used by these authors is not as efficient as the basin-hopping method used in the present work, in particular it may miss some very important geometries resulting from global structural changes such as the anti-Mackay/Mackay transition. In order to estimate the possible failures of the growth algorithm in Ref. 61, we also optimized the neutral clusters by basin-hopping, with the same number of quenches as for the cations. We did not find any difference with the work of Poteau and Spiegelmann except for large clusters $n>34$. Hence the geometries of clusters containing up to 34 atoms is significantly influenced by the electron count. The comparison between the neutral and charged clusters containing more than about 20 atoms shows that the occurrence of a capped double icosahedron and of anti-Mackay geometries becomes general for both charge states. In the range up to $n=39$ atoms, only some qualitative differences remain between the structures of Na_n and $\mathrm{Na}_n{}^+$, but they still involve anti-Mackay geometries.

The structures found in the semiclassical extended-Thomas-Fermi model are represented on Fig. 1(c). This density-based model treats explicitly the continuous background of valence electrons; however, it misses quantal fluctuations associated with the electronic shell structure which can be restored only with a more realistic kinetic energy description, actually with explicit orbitals as in the Kohn-Sham scheme. As a consequence, it has a smooth size-dependent behavior which explains the lack of significant deviations in the upper part of Fig. 2. It is striking that many geometrical configurations presented in Fig. 1(c) are the same as those obtained using the empirical SMA potential. In particular, the only sizes above 8 where the ETF and TB geometries are identical are 26, 29, and 30. Moreover, the energies of isomers which correspond to the global minima in the SMA potential are very close to the ground state energies, as seen from Table I. Thus, we found the icosahedral and anti-Mackay growth sequences to be dominant in the size range $4\leqslant n\leqslant 40$. We also found the hexagonal elements at $n=16$, but also at $n=15$, 17, and 22. The truncated octahedron is close to the lowest-energy structure at $n=38$ only, but we found two Mackay-type geometries for $n=39$ and 40 already obtained with the SMA potential. Similar morphologies induce similar stabilities, as can be inferred from Fig. 2(b). The same secondary magic numbers are found with the ETF model as with the SMA model, that characterize the anti-Mackay sequence: $n=13$, 19, 23, and 26. The peaks are however less marked in the ETF model, and no special stability can be guessed for $\mathrm{Na}_{29}{}^+$ from Fig. 2(b), although a distinct peak is observed for $n=32$.

In addition to the energetic quantities presented in Fig. 2, we have investigated some geometric features of the clusters in the three models. For this, we have calculated the Hill-Wheeler parameters r_c, β, and γ well known in nuclear physics. These parameters provide a global information on the average shape of a given cluster. The root-mean-square radius r_c is defined by

$$r_c=\left(\frac{1}{n}\sum_{i=1}^{n} r_i^2\right)^{1/2}. \tag{18}$$

The evaluation of r_c according to Eq. (18) requires that the cluster center of mass is located at the origin of a reference frame. The shape parameters β and γ are related to the principal momenta of inertia $I_1\geqslant I_2\geqslant I_3\geqslant 0$ via the expression

TABLE I. Binding energies (in eV) and point group (PG) of all clusters found in the three models. For each size, the lowest energy is in bold face.

Size	SMA	TB	ETF	PG
4	−**2.797**	—	−**3.730**	T_d
4	—	−**1.926**	—	D_{2h}
5	−**3.524**	−**2.765**	−**4.715**	D_{3h}
6	−**4.335**	—	−**5.698**	O_h
6	—	−**3.412**	—	C_{2v}
7	−**5.099**	−**4.471**	−**6.669**	D_{5h}
8	−**5.861**	−5.037	−**7.616**	D_{2d}
8	—	−**5.088**	−7.499	C_s
9	−**6.661**	−6.035	−**8.585**	C_{2v}
9	−6.631	−**6.174**	−8.563	D_{3h}
10	−**7.494**	−6.715	−**9.553**	C_{3v}
10	−7.382	−**6.775**	−9.551	C_{3v}
11	−**8.318**	−7.461	−**10.519**	C_{2v}
11	−8.122	−**7.714**	−10.517	D_{3h}
12	−**9.227**	−8.177	−**11.529**	C_{5v}
12	−8.990	−**8.313**	−11.526	C_s
13	−**10.212**	−8.982	−**12.601**	I_h
13	−9.749	−**9.243**	−12.598	C_{3v}
14	−**10.960**	−9.847	−**13.512**	C_{3v}
14	−10.808	−**9.945**	−13.507	C_s
15	−**11.790**	−10.813	−14.370	C_{2v}
15	−11.578	−**10.911**	−14.476	C_s
15	−11.768	−10.830	−**14.484**	D_{6d}
16	−**12.623**	−11.556	−**15.436**	C_s
16	−12.481	−**11.714**	−15.434	C_s
17	−**13.464**	−12.615	−16.380	C_{3v}
17	−13.455	−**12.677**	−16.386	C_s
17	−13.401	−12.334	−**16.397**	T_d
18	−**14.359**	−13.532	−17.376	C_{5v}
18	−14.296	−**13.545**	−17.374	C_1
18	−14.318	−13.464	−**17.379**	C_s
19	−**15.303**	−14.522	−**18.451**	D_{5h}
19	−15.200	−**14.544**	−18.448	C_s
20	−**16.149**	−15.327	−**19.403**	C_{2v}
20	−16.038	−**15.371**	−19.401	C_s
21	−**16.995**	−16.293	−**20.356**	C_{2v}
21	−16.873	−**16.353**	−20.350	C_s
22	−**17.880**	−17.074	−21.333	C_s
22	−17.836	−**17.145**	−21.335	C_{2v}
22	−17.801	−16.900	−**21.352**	D_{6h}
23	−**18.843**	−18.035	−**22.383**	D_{3h}
23	−18.661	−**18.092**	−22.304	C_{3v}
24	−**19.684**	−18.927	−23.324	C_s
24	−19.616	−**18.930**	−23.335	C_s
24	−19.678	−18.865	−**23.338**	C_s
25	−**20.579**	−**19.918**	−24.309	C_s
25	−20.508	−19.918	−**24.323**	C_3
26	−**21.550**	−**20.788**	−**25.346**	T_d
27	−**22.388**	−**21.648**	26.298	C_{2v}
27	−22.350	−21.501	−**26.320**	C_{2v}
28	−**23.273**	−**22.519**	−27.248	C_1
28	−23.259	−22.266	−**27.338**	T
29	−**24.236**	−**23.583**	−**28.328**	D_{3h}
30	−**25.074**	−24.299	−29.253	C_{2v}
30	−25.069	−**24.356**	−**29.275**	C_1
31	−**25.947**	−**25.278**	−30.260	C_s
31	−25.928	−25.167	−**30.274**	C_s
32	−**26.913**	−**26.176**	−31.297	C_{2v}
32	−26.845	−25.893	−**31.338**	C_3
33	−**27.803**	−**27.147**	−32.252	C_s
33	−27.719	−26.783	−**32.279**	C_1
34	−**28.761**	−**28.002**	−33.286	D_{5h}
34	−28.739	−27.882	−**33.316**	C_1
35	−**29.626**	−28.677	−**34.309**	C_3
35	−29.545	−**28.911**	−34.214	C_s
36	−**30.492**	−29.373	−**35.291**	C_2
36	−30.489	−**29.697**	−35.212	C_s
37	−**31.449**	−30.535	−36.252	C_3
37	−31.419	−**30.687**	−36.244	C_s
37	−31.373	−30.434	−**36.301**	C_1
38	−**32.372**	−30.875	−37.294	T_h
38	−32.285	−**31.496**	−37.248	C_s
38	−32.339	−31.302	−**37.305**	C_5
39	−**33.313**	−32.296	−**38.363**	C_{5v}
39	−33.218	−**32.459**	−38.173	C_1
40	−**34.187**	−33.036	−**39.318**	C_{2v}
40	−34.173	−**33.302**	−39.294	C_s

$$I_k=\frac{2}{3}r_c^2\left[1+\beta\sin\left(\gamma+\frac{(4k-3)\pi}{6}\right)\right],\quad k=1,2,3. \quad (19)$$

β lies in the range $0\leqslant\beta\leqslant 1$, and is a measure of the cluster oblateness. γ is in the range $0\leqslant\gamma\leqslant\pi/3$, and measures the cluster triaxiality. A zero value for β means a spherical shape, while $(0\leqslant\beta\leqslant 1,\ \gamma=0)$ defines an axially symmetric prolate ellipsoid and $(0\leqslant\beta\leqslant 1/2,\ \gamma=\pi/3)$ defines an axially symmetric oblate ellipsoid.

The variations of the parameters r_c, β, and γ are represented on Fig. 3 as function of the cluster size. From the top most panel of Fig. 3 we observe that the three models used predict different average ionic densities: for all sizes except for $Na_4{}^+$ (TB), ETF clusters are bigger than SMA clusters, which are, in turn, bigger than TB clusters. This finding is consistent with the ordering of the equilibrium bond length R_e of the dimer Na_2 in the three models: $R_e=6.73a_0$ in the ETF model, $6.32a_0$ in the SMA model, and $5.82a_0$ in the TB model. However the two former models were not expected to be accurate for very small clusters, whereas, on the contrary, the TB model might not be flexible enough to correctly account for the nearest-neighbor distance increase between the dimer and the bulk. In Fig. 3(a), we also observe some deviations with respect to the continuous law $N^{1/3}$ for some highly non-spherical configurations such as of $Na_{14}{}^+$ (SMA). Nonsphericity is better reflected by the parameter β, whose variations with the size are shown in Fig. 3(b). Because of the strong similarity between the SMA and ETF morphologies, we see mainly two different variations of β with the size, either with the SMA/ETF or TB models. In classical or semiclassical models, many clusters appear as rather spheri-

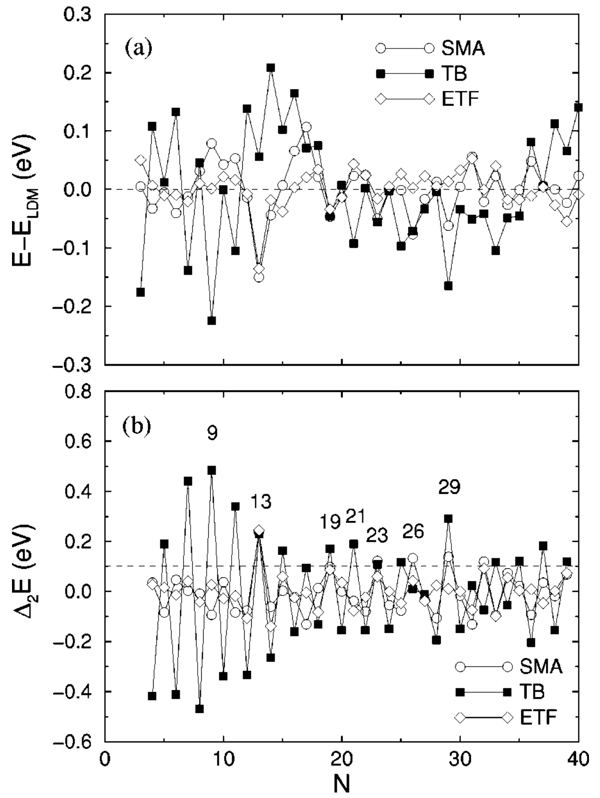

FIG. 2. Energetic stabilities of the clusters in the three models. (a) Relative energies are given with respect to the liquid-drop model energy $E_{\mathrm{LDM}}(N)$. (b) $\Delta_2E(N)$. All energies are expressed in eV. The best fits for the liquid drop energies were obtained with the following values of the parameters: $E_{\mathrm{LDM}}^{\mathrm{SMA}}(N)=-0.603\,79+0.200\,10N^{1/3}+0.703\,92N^{2/3}-1.0631N$; $E_{\mathrm{LDM}}^{\mathrm{TB}}(N)=-0.56079+0.097\,74N^{1/3}+0.403\,52N^{2/3}-1.0250N$; $E_{\mathrm{LDM}}^{\mathrm{ETF}}(N)=0.507\,19-0.078\,66N^{1/3}+0.497\,94N^{2/3}-1.0544N$.

cal. The highly symmetric $\mathrm{Na_4}^+$, $\mathrm{Na_6}^+$, $\mathrm{Na_{13}}^+$, $\mathrm{Na_{17}}^+$, $\mathrm{Na_{26}}^+$, $\mathrm{Na_{28}}^+$, and $\mathrm{Na_{34}}^+$ clusters, in both the ETF and SMA models, as well as $\mathrm{Na_{38}}+$ (SMA), have very low values of β. On the contrary, some sizes exhibit a significant nonspherical character in these models, such as $\mathrm{Na_5}^+$, $\mathrm{Na_7}^+$, $\mathrm{Na_{14}}^+$, or $\mathrm{Na_{19}}^+$. In the tight-binding model, only $\mathrm{Na_{26}}^+$ seems to be spherical, but it has the same geometry as in the other models.

Not much information provides a triaxiality shape parameter γ displayed in Fig. 3(c). This is mainly due to the high sensitivity of this quantity with respect to small distortions. This is a particular problem in the ETF model, where the optimization had to be made within some uncertainty on the energy, resulting in some uncertainty on the ionic geometry. In the SMA model, most clusters exhibit either very small ($\gamma\sim0$) or very large ($\gamma\sim\pi/3$) values of γ, suggesting axially symmetric configurations. The only notable triaxial clusters (having also reasonably large values of β) in this model are found for $n=11$, 22, 30–32. The tight-binding model predicts usually a larger number of triaxial shapes, including $n=6$, 8, 12, 14, 17–22, 24, 25, 30–33, and 35–40. Indeed, as can be seen from Fig. 3(c), only a few structures are axially symmetric in average in this model.

The geometric parameters investigated demonstrate the basic propensity of the tight-binding model to yield strongly size-dependent ionic morphologies. The quantal effects present in this model are therefore extremely important in the complete size range $n\leqslant40$. Consequences in terms of the dynamics could be also of a major importance, because not only the lowest-energy isomer but also the complete energy landscape should be affected by the differences observed. As a matter of fact, some of these differences have been observed from the thermodynamic behavior in a few selected cases.[41] Conversely, the general similarity between the classical SMA and semiclassical ETF models suggests similar energy landscapes, and hence a qualitatively similar thermodynamic behavior. Recent theoretical investigations seem to confirm the present hypothesis.[71]

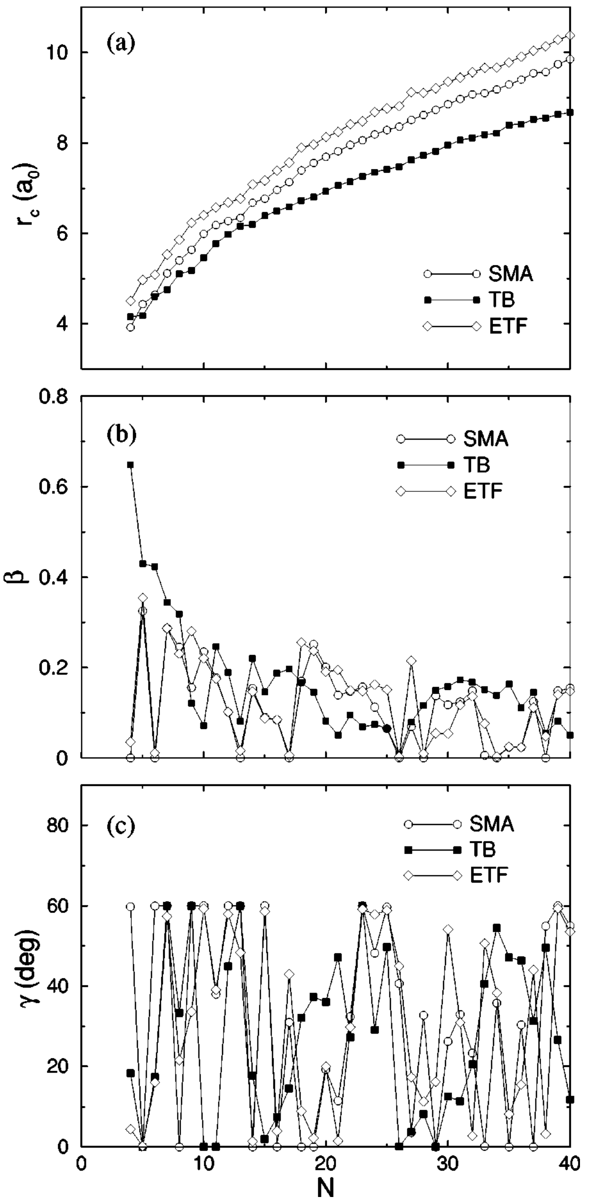

FIG. 3. Hill-Wheeler shape parameters r_c, β, and γ for all the clusters in the three models. (a) Average radius r_c in atomic units; (b) sphericity parameter β; (c) triaxiality parameter γ in degrees.

IV. CONCLUSION

We have investigated geometrical properties of medium size cationic sodium clusters $\mathrm{Na}_n{}^+$ for $n\leqslant40$. Three model potentials were used to describe the metallic bonding. First, a many-body empirical potential of the embedded-atom family was modified to account for the extra ionic charge. A distance-dependent tight-binding model was also used as one of the most simple quantal model. At last, a semiclassical DFT-based orbital-free model was used. In the range of sizes investigated here, all these models keep a reasonable computational cost which allows for extensive and unconstrained global optimizations. We have chosen the ‘‘basin-hopping’’ method of Wales and Doye for the two first potentials, but in the case of the semiclassical potential, we had to adopt a ‘‘semiglobal’’ optimization approach starting from databases of putative lowest-energy configurations.

The geometries obtained with the TB model are generally different from those obtained with the classical and semiclassical potentials. For small cluster ions, $n=2$–9, 11, and 21, configuration-interaction (CI) calculations based on Hartree-Fock gradient optimization are available.[9] All TB structures are in agreement with the CI results except for two cases. For $n=5$, the TB model yields a bipyramid. The lowest CI structure has D_{2d} symmetry, and consists of two twisted triangles sharing one apex atom. For $n=9$, the CI structure consists of two twisted rhombus superimposed with an extra atom capping the upper rhombus. The present TB structure is closely connected to this CI geometry, and only differs via the medium section which is a square instead of a rhombus. The D_{2d} TB structure is also very close to the CI C_s structure. One should notice that, for $n=4$, 6–9, and 11, agreement is also reached with the results of unrestricted quantum molecular dynamics.[72] The latter work involves approximations of the time-dependent LDA equations which were derived in order to study a cluster-atom charge transfer. This agreement reflects the more realistic quantal effects exhibited by the TB model, accounting, in particular, for Jahn-Teller deformations, examplified for $n=13$. One should also notice the stronger effect of charging the cluster (the other models do not show such a structural dependence) which was also found in *ab initio* calculations involving ionic structures.[8,9] Below the 15-ion size, the TB model does not provide any particular growth sequence, while above this size, pentagonal and icosahedral elements become usual. These elements are clearly displayed by the classical and semiclassical models even for smaller sizes. In particular, the growth sequence of an icosahedron (for $n=13$) appears to be similar to the growth of Lennard-Jones clusters. An interesting property of these two models is that they exhibit some hexagonal elements for several sizes. In the semiclassical model, $\mathrm{Na_{22}}^+$ has even D_{6h} symmetry.

A wide range ($n=7$–55) of odd clusters have also been investigated with the CAPS formalism.[8] In the range 7–21, similarities are found with the present results. In particular, the occurence of low energy structures showing an irregular growth sequence around a single icosahedron beyond $n=15$ towards the double icosahedron. This latter structure was found as the lowest isomer of $\mathrm{Na_{19}}^+$ in CAPS calculations. The CAPS results however differ significantly from those obtained by all models applied here for $n\geqslant 25$. Indeed, Kümmel *et al.*[8] found $\mathrm{Na_{25}}^+$ to be an essentially prolate triple icosahedron (axial cluster having four pentagonal rings and five atoms on the axis), also seen as the building block for the growth sequence in the range 25–55. This sequence correlates with the finding of a fivefold symmetric two-body structure for $\mathrm{Na_{43}}^+$ with an extremely strong octupole deformation. The influence of the CAPS constraint in this range should however be checked. On the other hand, the three models applied here, including the tight-binding model, show structures built around one or several intricated double icosahedra, not exhibiting such large deformations.

The global analysis of geometrical configurations obtained was made with the Hill-Wheeler parameters r_c, β, and γ. Values of the oblateness parameter β have shown that many sizes can be considered as spherical in the classical and semiclassical models, but not in the TB model where only $\mathrm{Na_{26}}^+$ is spherical. Unfortunately, the amplitude of variations of the triaxiality parameter γ are very large, which makes the interpretation difficult. However, we have observed that the general trend of the TB model is to predict triaxial structures, whereas the classical and semiclassical models favor axisymmetric shapes.

An application of a semiglobal approach was very instructive in the present case, because it turns out that the classical and semiclassical models predict very similar ionic structures in the whole range $n=4$–40. Indeed, this similarity is not surprising because the semiclassical ETF model can be considered as an embedded-atom version of the quantal Kohn-Sham density-functional theory, in the same way as the empirical SMA potential is an approximation of the quantal tight-binding model. This feature could be used to analyze the microscopic aspects of melting of ETF clusters in terms of regular quenches performed using the SMA potential. In this purpose, a better fit between these two models could be obtained following the suggestion of Hartke[73] to simultaneously globally optimize the geometries in the semiclassical potential while fitting the parameters of a classical potential over configurations of an accumulated database.

The present results show that only the TB model is physically relevant with respect to more sophisticated studies in the range $n<20$. This model includes orbital effects which yield important features such as the odd/even alternations in the stabilities or Jahn-Teller deformations. It also provides the main magic stabilities at $n=9$, 19, and 21, although the shell effects are not explicitely accounted for. The two other models are unable to reproduce these properties. In the large size range, the impact of the detailed electronic structure is expected to be less important, and the description of metallic bonding by the SMA and ETF models should become more realistic. We then expect these models to be useful as guidelines for optimization of clusters containing more than a hundred atoms.

[*] Electronic address: fcalvo@cea.fr

[1] W. D. Knight, K. Clemenger, W. A. de Heer, W. A. Saunders, M. Y. Chou, and M. L. Cohen, Phys. Rev. Lett. **52**, 2141 (1984).

[2] W. A. de Heer, Rev. Mod. Phys. **65**, 611 (1993).

[3] M. Brack, Rev. Mod. Phys. **65**, 677 (1993).

[4] *Nuclear Aspects of simple Metal Clusters*, edited by C. Bréchignac and Ph. Cahuzac, Comments At. Mol. Phys. **31**, Nos. 3–6.

[5] D. E. Beck, Solid State Commun. **49**, 381 (1984).

[6] W. Eckardt, Phys. Rev. B **29**, 1558 (1984).

[7] J. M. Pacheco and J. L. Martins, J. Chem. Phys. **106**, 6039 (1997).

[8] S. Kümmel, M. Brack and P.-G. Reinhardt, Phys. Rev. B **62**, 7602 (2000).

[9] V. Bonačić-Koutecký, J. Pittner, C. Fuchs, P. Fantucci, M. F. Guest, and J. Koutecký, J. Chem. Phys. **104**, 1427 (1996).

[10] M. Schmidt, R. Kusche, W. Kronmüller, B. von Issendorff, and H. Haberland, Phys. Rev. Lett. **79**, 99 (1997); M. Schmidt, B. Kusche, B. von Issendorff, and H. Haberland, Nature (London) **393**, 238 (1998).

[11] P. Fantucci and J. Koutecký, in *Elemental and Molecular Clusters*, edited by G. Benedek, T. P. Martin, and G. Pacchioni (Springer, Berlin, 1988), p. 125.

[12] V. Bonačić-Koutecký, P. Fantucci, and J. Koutecký, Chem. Rev. **91**, 1035 (1991).

[13] J. L. Martins, J. Buttet, and R. Car, Phys. Rev. B **31**, 1804 (1985).

[14] U. Röthlisberger and W. Andreoni, J. Chem. Phys. **94**, 8129 (1991).

[15] G. Gardet, F. Rogemond, and H. Chermette, J. Chem. Phys. **105**, 9933 (1993).

[16] F. Spiegelmann and D. Pavolini, J. Chem. Phys. **89**, 4954 (1988).

[17] I. Andricioaei and J. E. Straub, J. Chem. Phys. **107**, 9117 (1997).

[18] P. K. Venkatesh, M. H. Cohen, R. W. Carr, and A. M. Dean, Phys. Rev. E **55**, 6219 (1997).

[19] H. Xu and B. J. Berne, J. Chem. Phys. **112**, 2701 (2000).

[20] D. B. Faken, A. F. Voter, D. L. Freeman, and J. D. Doll, J. Phys. Chem. A **103**, 9521 (1999).

[21] J. P. K. Doye, D. J. Wales, and R. S. Berry, J. Chem. Phys. **103**, 4234 (1995).

[22] R. H. Leary and J. P. K. Doye, Phys. Rev. E **60**, R6320 (1999).

[23] D. J. Wales and J. P. K. Doye, J. Phys. Chem. A **101**, 5111 (1997).

[24] D. M. Deaven, N. Tit, J. R. Morris, and K. M. Ho, Chem. Phys. Lett. **256**, 195 (1996); M. D. Wolf and U. Landmann, J. Phys. Chem. A **102**, 6129 (1998); B. Hartke, J. Comput. Chem. **20**, 1752 (1999).

[25] W. Eckardt and Z. Penzar, Phys. Rev. B **38**, 4273 (1988); Z. Penzar and W. Eckardt, Z. Phys. D: At., Mol. Clusters **17**, 69 (1990).

[26] G. Lauritsch, P.-G. Reinhardt, and J. Meyer, Z. Phys. D: At., Mol. Clusters **32**, 125 (1994).

[27] G. Lauritsch, P.-G. Reinhardt, and J. Meyer, Phys. Lett. A **160**, 179 (1991).

[28] S. Kasperl, C. Kohl, and P.-G. Reinhardt, Phys. Lett. A **206**, 179 (1995).

[29] B. Montag, Th. Hirschmann, J. Meyer, P.-G. Reinhardt, and M. Brack, Phys. Rev. B **52**, 4775 (1995).

[30] C. Yannouleas and U. Landman, Phys. Rev. B **48**, 8376 (1993); Chem. Phys. Lett. **210**, 437 (1993).

[31] C. Yannouleas and U. Landman, Phys. Rev. B **51**, 1902 (1995).

[32] C. Yannouleas and U. Landman, in *Large Clusters of Atoms and Molecules, NATO ASI Series E: Applied Sciences*, edited by T. P. Martin (Kluwer, Dordrecht, 1996), Vol. 313, p. 131.

[33] C. Yannouleas and U. Landman, Phys. Rev. Lett. **78**, 1424 (1997).

[34] M. P. Iñiguez, J. A. Alonso, and L. C. Balbás, Solid State Commun. **57**, 85 (1986).

[35] B. Montag and P.-G. Reinhardt, Phys. Lett. A **193**, 380 (1994).

[36] B. Montag and P.-G. Reinhardt, Z. Phys. D: At., Mol. Clusters **33**, 265 (1995).

[37] L. Girifalco and V. Weizer, Phys. Rev. **114**, 687 (1959).

[38] P. Blaise, S. A. Blundell, and C. Guet, Phys. Rev. B **55**, 15 856 (1997).

[39] See for instance A. Dhavale, V. Shah, and D. G. Kanhere, Phys. Rev. A **57**, 4522 (1998); Y. A. Wang, N. Govind, and E. A. Carter, Phys. Rev. B **58**, 13 465 (1998); A. Aguado, J. M. López, J. A. Alonso, and M. J. Stott, J. Chem. Phys. **111**, 6026 (1999), and references therein.

[40] F. Calvo and F. Spiegelmann, Phys. Rev. Lett. **82**, 2270 (1999).

[41] F. Calvo and F. Spiegelmann, J. Chem. Phys. **112**, 2888 (2000).

[42] M. B. Gordon, F. Cyrot-Lackmann, and M. C. Desjonqueres, Surf. Sci. **80**, 159 (1979); R. P. Gupta, Phys. Rev. B **23**, 6265 (1981); D. Tománek, S. Mukherjee, and K. H. Bennemann, *ibid.* **28**, 665 (1983).

[43] A. F. Voter and S. P. Chen, in *Characterization of Defects in Materials*, edited by R. W. Siegal, J. R. Weertman, and R. Sinclair, MRS Symposia Proceedings No. 82 (Materials Research Society, Pittsburgh, 1987), p. 175; M. S. Daw and M. I. Baskes, Phys. Rev. Lett. **50**, 1285 (1983); Phys. Rev. B **29**, 6443 (1984).

[44] F. Ducastelle, J. Phys. (Paris) **31**, 1055 (1970).

[45] S. Sawada and S. Sugano, Z. Phys. D: At., Mol. Clusters **12**, 189 (1989); **14**, 247 (1989); **20**, 259 (1991).

[46] C. Rey, L. J. Gallego, J. García-Rodeja, J. A. Alonso, and M. P. Iñiguez, Phys. Rev. B **48**, 8253 (1993).

[47] A. Bulgac and D. Kusnezov, Phys. Rev. Lett. **68**, 1335 (1992); Phys. Rev. B **45**, 1988 (1992).

[48] N. Ju and A. Bulgac, Phys. Rev. B **48**, 2721 (1993).

[49] M. Fosmire and A. Bulgac, Phys. Rev. B **52**, 17 509 (1995).

[50] M. I. Baskes, Phys. Rev. Lett. **83**, 2592 (1999).

[51] Y. Li, E. Blaisten-Barojas, and D. A. Papaconstantopoulos, Phys. Rev. B **57**, 15 519 (1998); Chem. Phys. Lett. **268**, 331 (1997).

[52] C. Bréchignac, Ph. Cahuzac, J. Leygnier, and J. Weiner, J. Chem. Phys. **90**, 1492 (1989).

[53] M. M. Kappes, M. Schär, U. Röthlisberger, C. Yeretzian, and E. Schumacher, Chem. Phys. Lett. **143**, 251 (1988).

[54] M. L. Homer, J. L. Persson, E. C. Honea, and R. L. Whetten, Z. Phys. D: At., Mol. Clusters **22**, 441 (1991).

[55] F. Calvo, Phys. Rev. B **60**, 15 601 (1999).

[56] The value of ε_0 has been given uncorrectly in Refs. 40, 41, and 55.

[57] M. J. López and J. Jellinek, J. Chem. Phys. **110**, 8899 (1999).

[58] J. P. K. Doye and D. J. Wales, New J. Chem. **22**, 733 (1998); Phys. Rev. B **59**, 2292 (1999); D. J. Wales and M. P. Hodges, Chem. Phys. Lett. **286**, 65 (1998); F. Calvo, G. Torchet, and M.-F. de Feraudy, J. Chem. Phys. **111**, 4650 (1999).

[59] W. Wenzel and K. Hamacher, Phys. Rev. Lett. **82**, 3003 (1999).

[60] R. Poteau and F. Spiegelmann, Phys. Rev. B **45**, 1878 (1991).

[61] R. Poteau and F. Spiegelmann, J. Chem. Phys. **98**, 6540 (1993).

[62] A. Goerke, H. Palm, C. P. Schulz, F. Spiegelmann, and I. V. Hertel, J. Chem. Phys. **98**, 9635 (1993).

[63] A. Bulgac and C. Lewenkopf, Europhys. Lett. **31**, 519 (1995).

[64] R. Poteau, F. Spiegelmann, and P. Labastie, Z. Phys. D: At., Mol. Clusters **30**, 57 (1994).

[65] F. Calvo and F. Spiegelmann, Phys. Rev. B **54**, 10 949 (1996).

[66] V. Bonačić-Koutecký, P. Fantucci, and J. Koutecký, Phys. Rev. B **37**, 4369 (1988); V. Bonačić-Koutecký, I. Boustani, M. Guest, and J. Koutecký, J. Chem. Phys. **89**, 4861 (1988).

[67] R. Poteau and F. Spiegelmann, Comments At. Mol. Phys. **31**, 395 (1995).

[68] O. Gunnarsson and B. I. Lundqvist, Phys. Rev. B **13**, 4274 (1976).

[69] I. L. Garzón, K. Michaelian, M. R. Beltrán, A. Posada-Amarillas, P. Ordejón, E. Artacho, D. Sánchez-Portal, and J. M. Soler, Phys. Rev. Lett. **81**, 1600 (1998).

[70] E. K. Parks, G. C. Nieman, K. P. Kerns, and S. J. Riley, J. Chem. Phys. **107**, 1861 (1997).

[71] S. Tran, Ph.D. thesis, Grenoble University (2000).

[72] O. Knospe, J. Jellinek, U. Saalman, and R. Schmidt, Phys. Rev. A **61**, 022 715 (2000).

[73] B. Hartke, Chem. Phys. Lett. **258**, 144 (1996).